Journal of Pathology
J Pathol November 2021; **255:** 243–256
Published online 26 August 2021 in Wiley Online Library (wileyonlinelibrary.com) DOI: 10.1002/path.5772

ORIGINAL PAPER

Infiltration of NK and plasma cells is associated with a distinct immune subset in non-small cell lung cancer

Max Backman[1†], Linnéa La Fleur[1†], Pinja Kurppa[1], Dijana Djureinovic[1], Hedvig Elfving[1], Hans Brunnström[2], Johanna Sofia Margareta Mattsson[1], Amanda Lindberg[1], Victor Pontén[1], Mohamed Eltahir[3], Sara Mangsbo[3], Miklos Gulyas[1], Johan Isaksson[1,4], Karin Jirström[5], Klas Kärre[6], Karin Leandersson[7], Artur Mezheyeuski[1], Fredrik Pontén[1], Carina Strell[1], Cecilia Lindskog[1], Johan Botling[1‡*] and Patrick Micke[1‡*]

[1] *Department of Immunology, Genetics and Pathology, Uppsala University, Uppsala, Sweden*
[2] *Division of Pathology, Lund University, Skåne University Hospital, Lund, Sweden*
[3] *Department of Pharmaceutical Bioscience, Uppsala University, Uppsala, Sweden*
[4] *Department of Respiratory Medicine, Gävle Hospital, Gävle, Sweden*
[5] *Division of Oncology and Therapeutic Pathology, Department of Clinical Sciences Lund, Lund, Sweden*
[6] *Department of Microbiology, Cell and Tumor Biology, Karolinska Institutet, Stockholm, Sweden*
[7] *Cancer Immunology, Department of Translational Medicine, Lund University, Skånes University Hospital, Malmö, Sweden*

**Correspondence to: P Micke or J Botling, Department of Immunology, Genetics and Pathology, Uppsala University, 751 85 Uppsala, Sweden. E-mail: patrick.micke@igp.uu.se (P Micke) or johan.botling@igp.uu.se (J Botling)*

[†]Equal contributions.
[‡]Co-senior authors.

Abstract

Immune cells of the tumor microenvironment are central but erratic targets for immunotherapy. The aim of this study was to characterize novel patterns of immune cell infiltration in non-small cell lung cancer (NSCLC) in relation to its molecular and clinicopathologic characteristics. Lymphocytes (CD3+, CD4+, CD8+, CD20+, FOXP3+, CD45RO+), macrophages (CD163+), plasma cells (CD138+), NK cells (NKp46+), PD1+, and PD-L1+ were annotated on a tissue microarray including 357 NSCLC cases. Somatic mutations were analyzed by targeted sequencing for 82 genes and a tumor mutational load score was estimated. Transcriptomic immune patterns were established in 197 patients based on RNA sequencing data. The immune cell infiltration was variable and showed only poor association with specific mutations. The previously defined immune phenotypic patterns, desert, inflamed, and immune excluded, comprised 30, 13, and 57% of cases, respectively. Notably, mRNA immune activation and high estimated tumor mutational load were unique only for the inflamed pattern. However, in the unsupervised cluster analysis, including all immune cell markers, these conceptual patterns were only weakly reproduced. Instead, four immune classes were identified: (1) high immune cell infiltration, (2) high immune cell infiltration with abundance of CD20+ B cells, (3) low immune cell infiltration, and (4) a phenotype with an imprint of plasma cells and NK cells. This latter class was linked to better survival despite exhibiting low expression of immune response-related genes (e.g. *CXCL9*, *GZMB*, *INFG*, *CTLA4*). This compartment-specific immune cell analysis in the context of the molecular and clinical background of NSCLC reveals two previously unrecognized immune classes. A refined immune classification, including traits of the humoral and innate immune response, is important to define the immunogenic potency of NSCLC in the era of immunotherapy.

Keywords: immune cell infiltration; PD-L1; checkpoint therapy; tumor microenvironment; lung cancer; NSCLC; p53

Received 6 May 2021; Revised 13 July 2021; Accepted 28 July 2021

Conflict of interest statement: KL is a board member of Cantargia AB, a company developing IL1RAP inhibitors. This does not alter the author's adherence to all guidelines for publication and does not constitute a conflict of interest. No other potential conflicts of interest were declared.

Introduction

The introduction of checkpoint inhibitors has revolutionized lung cancer therapy and proved that the immune system can control cancer growth. Antibodies directed against the immune regulatory elements PD1 and PD-L1 are now approved in first- or second-line treatment [1]. However, most patients do not achieve long-term benefit, as a durable response has only been demonstrated in approximately 20% of patients [2–4]. Translational biomarker analyses suggest several parameters that have a predictive impact on PD1/PD-L1 therapy, yet the most convincing predictive marker is the immunohistochemical (IHC) expression of PD-L1 on cancer

cells [2–6]. Although numerous studies have found such an association, the predictive value is only moderate and varies considerably between studies [6]. Additional molecular biomarkers have been suggested, for example, tumor infiltrating lymphocytes, tumor mutation burden (TMB), and circulating tumor DNA [7–9]. These are now under evaluation, and some may soon enter clinical diagnostics.

A more complex, but promising, concept is based on the individual immune response patterns assessed by the abundance of different immune cells in a patient's tumor lesion [7,10,11]. Some tumors exhibit a high number of infiltrating immune cells, particularly CD4+ and CD8+ lymphocytes [6,7,9]. Transcriptomic analysis revealed that these tumors also express proinflammatory cytokines, indicating a basic antitumor immune response, although not efficient enough to control tumor growth [6,9,12,13]. These tumors have been designated inflamed or hot. By contrast, tumors with a general low immune infiltration signature were designated as immune desert or cold tumors [9,14,15]. A third tumor category is characterized by an abundance of immune cells in the stroma only, but not infiltrating the cancer cell nests; a phenotype termed immune excluded. [9,16,17]

Table 1. Patient characteristics of the Uppsala cohort.

	No.	%
No. patients	357	100.0
Age (years)		
≥70	141	39.5
<70	216	60.5
Gender		
Male	176	49.3
Female	181	50.7
Smoking category		
Smokers	182	51.0
Ex-smokers (>1 year)	134	37.5
Never-smokers	41	11.5
Histology		
Squamous cell carcinoma	103	28.9
Adenocarcinoma	229	64.4
Large cell carcinoma	8	2.2
Adenosquamous	5	1.4
Sarcomatoid	3	0.8
Large cell neuroendocrine carcinoma	9	2.5
Stage (TNM 7)		
IA	146	40.9
IB	76	21.3
IIA	41	11.5
IIB	34	9.5
IIIA	50	14.0
IIIB	0	0.0
IV	10	2.8
Performance status (WHO)		
0	214	59.9
1	138	38.7
2	5	1.4
Treatment		
No adjuvant treatment	166	46.5
Adjuvant treatment	151	42.3
Neoadjuvant treatment	3	0.8
Adjuvant + neoadjuvant treatment	1	0.3
Missing data	36	10.1

Although the three subgroups, inflamed, excluded, and desert, are accepted as immunotherapy biomarkers, both the inter- and intra-heterogeneity of different cancer types, the variability of used biomarkers, as well as applied criteria, challenge the efforts to establish an immune-based classification of lung cancer [17–19]. Few studies have managed to link immune cell infiltration to the benefit of checkpoint inhibition in non-small cell lung cancer (NSCLC) patients. In a recent study that applied multiplex quantitative immunofluorescence, the presence of CD3+ cells was associated with a durable clinical response in NSCLC patients treated with checkpoint inhibitors [4]. Furthermore, the authors identified a dormant immune phenotype characterized by the presence of T cells with low proliferation (low Ki67) or low activation (low granzyme B) in the tumor compartment that was strongly associated with survival of treated patients. It should be noted that this study included only 36 NSCLC cases and was carried out retrospectively. Also, immune cell phenotypes can be confounded by patient selection bias, i.e. smoking status, mutation status, marker selection (PD-L1), or histologic subtype. Indeed, attempts to establish prognostic immune profiles, such as the immunoscore developed in colorectal cancer, have failed to provide clinically relevant information in NSCLC so far [11,20].

It is evident that there is a need to better understand the immune response in NSCLC in a holistic and unbiased manner. Here we analyzed multiparametric immune phenotypes in a comprehensively annotated NSCLC patient cohort in relation to both clinical and molecular parameters, including mutational status, TMB, as well as RNA expression data. The ultimate goal was to identify fundamental immune response patterns in NSCLC.

Materials and methods

Patient material

This study included 357 NSCLC patients treated surgically at Uppsala University Hospital between 2006 and 2010 [21]. Patient characteristics are shown in Table 1. Tissue microarrays (TMAs) with duplicate 1-mm cores were constructed using representative formalin-fixed paraffin-embedded tumor tissue blocks, as described previously [22]. The study was conducted in accordance with the Declaration of Helsinki and the Swedish Ethical Review Act (approved by the Ethical Review Board in Uppsala, #2012/532).

Molecular analysis

Genomic DNA was extracted either from fresh-frozen or paraffin-embedded tissue. Targeted deep sequencing was carried out for 352 of the 357 patients included in this study using the Haloplex system for target amplification (Agilent Technologies, Santa Clara, CA, USA).

The analysis included all coding exons of 82 lung cancer-related genes (see supplementary material, Table S1). Sequencing was performed and 125-bp paired-end reads obtained using the Illumina HiSeq 2500 platform (Illumina, San Diego, CA, USA). The reads were mapped to the reference genome (hg19) and identification of mutations was carried out as described previously [23]. The tumor mutational load (TML) was estimated by dividing the number of non-synonymous mutations in a sample by the size (0.47 Mb) of the sequenced genome.

Corresponding gene expression data were available for 197 patients (see supplementary material, Table S2) obtained by RNA sequencing (RNAseq), as described previously [24]. RNA was extracted from fresh-frozen tissue and prepared for sequencing using the Illumina TruSeq RNA Sample Prep Kit v2 with polyA selection (Illumina). The sequencing was carried out based on the standard Illumina RNAseq protocol, with a read length of 2×100 bases. The raw data, together with clinical information, are available on the gene expression omnibus with the accession number GSE81089.

Immunohistochemistry

IHC was carried out as previously described [24]. In brief, sections cut at 4 μm from tissue paraffin blocks were dried onto slides overnight at room temperature and then heated at 50 °C for approximately 12 h. Deparaffinization was carried out using xylene and hydration using consecutively weaker solutions of ethanol. During deparaffinization, blocking of endogenous peroxidase was accomplished by a 5-min exposure to 0.3% H_2O_2 in 95% ethanol. Heat-induced epitope retrieval was used as the antigen retrieval method, with 4 min of pressure boiling with a pH 6 retrieval buffer and subsequent cooling to 90 °C.

A full protocol is available on the website of the human protein atlas (http://www.proteinatlas.org/download/IHC_protocol.pdf). The antibodies used for the IHC analyses were as follows: CD3ε (CL1497, 1:1000 dilution; Atlas Antibodies, Stockholm, Sweden), CD4 (CL0395, 1:125 dilution; Atlas Antibodies), CD8A (CL1529, 1:250 dilution; Atlas antibodies), CD20 (L26, pre-prepared manufacturer dilution; Agilent Technologies), CD45RO (UCHL1, 1:1000 dilution; Abcam, Cambridge, UK), CD138 (MI15, 1:100 dilution; Agilent Technologies), CD163 (10D6, 1:100 dilution; Novocastra, Newcastle, UK), FOXP3 (236A/E7, 1:15 dilution; Santa Cruz Biotechnology, Dallas, TX, USA), PD1 (MRQ-22, 1:100 dilution; Cell Marque, Rocklin, CA, USA), and NKp46 (195314, 1:50 dilution; R&D Systems, Minneapolis, MN, USA).

PD-L1 (22C3, pre-prepared dilution; Agilent Technologies) staining was carried out at the Clinical Pathology Unit at Uppsala University Hospital on a DAKO autostainer system (Agilent Technologies) following the manufacturer's instructions, including antigen retrieval at pH6.

Annotation of immune cell infiltration

Immune marker-positive cells were visually annotated as the percentage of stained viable, nucleated cells in the respective stroma and tumor compartments for the whole tissue area of both TMA cores. The immune cell score in the stroma compartment was calculated by dividing positive immune cells by all immune cells and all other stroma cells (fibroblasts, endothelial cells, etc.). In the tumor compartment, the immune score was calculated by dividing positive immune cells by all other cells (tumor cells and immune cells). The increments used for visual annotation were 0, 1, 5, 10, 15, 20, 25, 30, 35, 40, 50, 60, 70, 80, 90, and 100%. The estimated percentage in each case was rounded down to the nearest increment and used as the immune marker score for further analysis. Thus, for example, if a quotient of 5% was annotated, approximately five of 100 viable cells in that compartment were stained in the corresponding compartment. For the annotation of the PD-L1 staining in the tumor compartment, we used the common annotation of cancer cell staining used in clinical diagnostics (tumor proportion score), which is the percentage of viable tumor cells showing partial or complete membrane staining (same percentage increments as above). The annotation for each marker was carried out by different observers (MB, PK, DD, HE, JSMM, ME) and supervised and reviewed by a trained lung pathologist (PM).

A different data set from the same patient cohort was used as part of a previous study describing immune cell infiltration in NSCLC [25]. The immunostains for CD3, CD4, CD8, FOXP3, and CD20 in that study were independently quantified using a different categorization and were annotated by different observers and not used in this study.

Immune classes based on CD8+ infiltration in tumor and stroma

Cases were divided into the immune classes inflamed, immune excluded, and immune desert based on CD8+ cell infiltration in the tumor and stroma compartments. Cases with ≥10% annotated CD8+ cells in the tumor compartment were classified as inflamed. Cases with <10% annotated CD8+ cells in the tumor compartment but ≥10% annotated CD8+ cells in the stroma compartment were classified as immune excluded. The remaining cases, having <10% of CD8+ cells in both tumor and stroma compartments, were classified as immune desert.

Statistics and bioinformatics

Difference in immune infiltrates between the two histologic subgroups (adenocarcinoma and squamous cell cancer) were analyzed using the Wilcoxon signed-rank test (see supplementary material, Table S3). A correlation analysis between immune markers as well as between immune markers and estimated TMB was carried out using Spearman's rank correlation (see supplementary material, Tables S4A–C

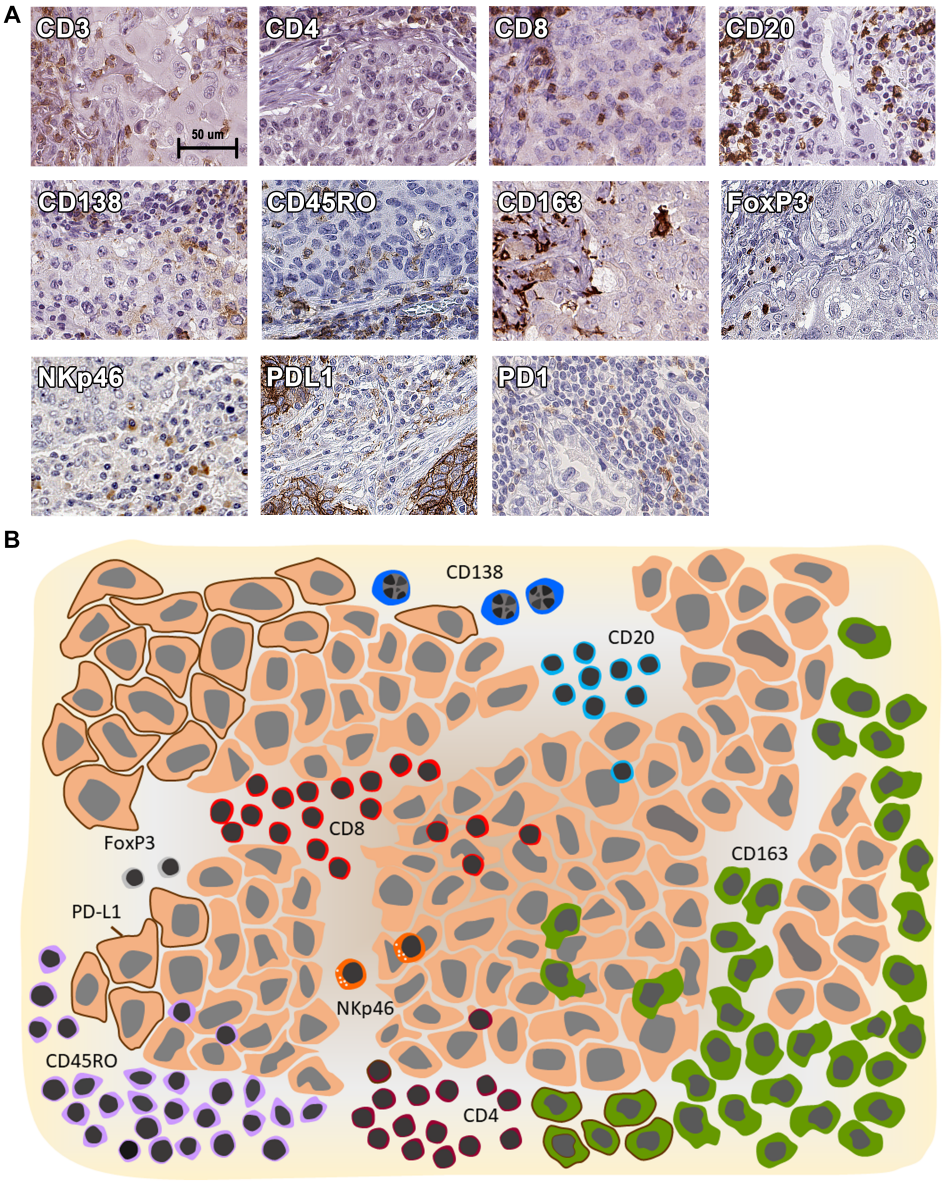

Figure 1. (A) Expression of immune markers in NSCLC tissue. Representative microscopic images of IHC staining of TMA sections including 357 NSCLC cases using antibodies against CD3, CD4, CD8, CD20, CD138, CD45RO, CD163, FOXP3, NKp46, PD1, and PD-L1. (B) The immune landscape of NSCLC. Illustration of the mean proportion of immune cell infiltration in the tumor cell compartment (orange large cells) and the stroma compartment (beige background). For visualization purposes the immune marker score was normalized to 100 cells. PD-L1 expression is displayed as a brown border in tumor cells. PD-L1 expression in the stroma and PD1 expression is not illustrated because it does not show cell type-specific expression and can be expressed by a variety of cells.

and S5A). Fisher's exact test was used to analyze relations between immune markers and mutations (see supplementary material, Table S5B–D). Comparisons between clinical data and immune infiltrates were assessed with the Wilcoxon signed-rank test (see supplementary material, Table S6). The association between immune classes (desert, immune excluded, and inflamed as well as inflamed, CD20, plasma NK, and desert) and estimated TML were carried out using the Wilcoxon signed-rank test (see supplementary material, Table S7A,B) and for histologic subtype Fisher's exact test was used (see supplementary material, Table S7C,D). Molecular differences between immune classes (desert, excluded, and inflamed, as well as the alternative immune classes proposed in this study, inflamed, CD20 inflamed, plasma NK, and desert) were analyzed using Fisher's exact test (see supplementary material, Table S8A,B). A survival analysis was carried out using multivariate Cox regressions controlling for stage, performance status, age, and smoking. The non-zero median was used as a cut-off to dichotomize the annotated marker ratios. A hierarchical cluster analysis was carried out with Euclidean distance as metric and complete-linkage clustering as the linkage criteria using the ComplexHeatmap package (version 1.99.0) for R [26] based on values for immune infiltrates and PD-L1 expression that were normalized. The survminer package (version 0.4.3.) was used to calculate pairwise comparisons between the four immune classes. The differential gene expression of the immune classes was compared using R package

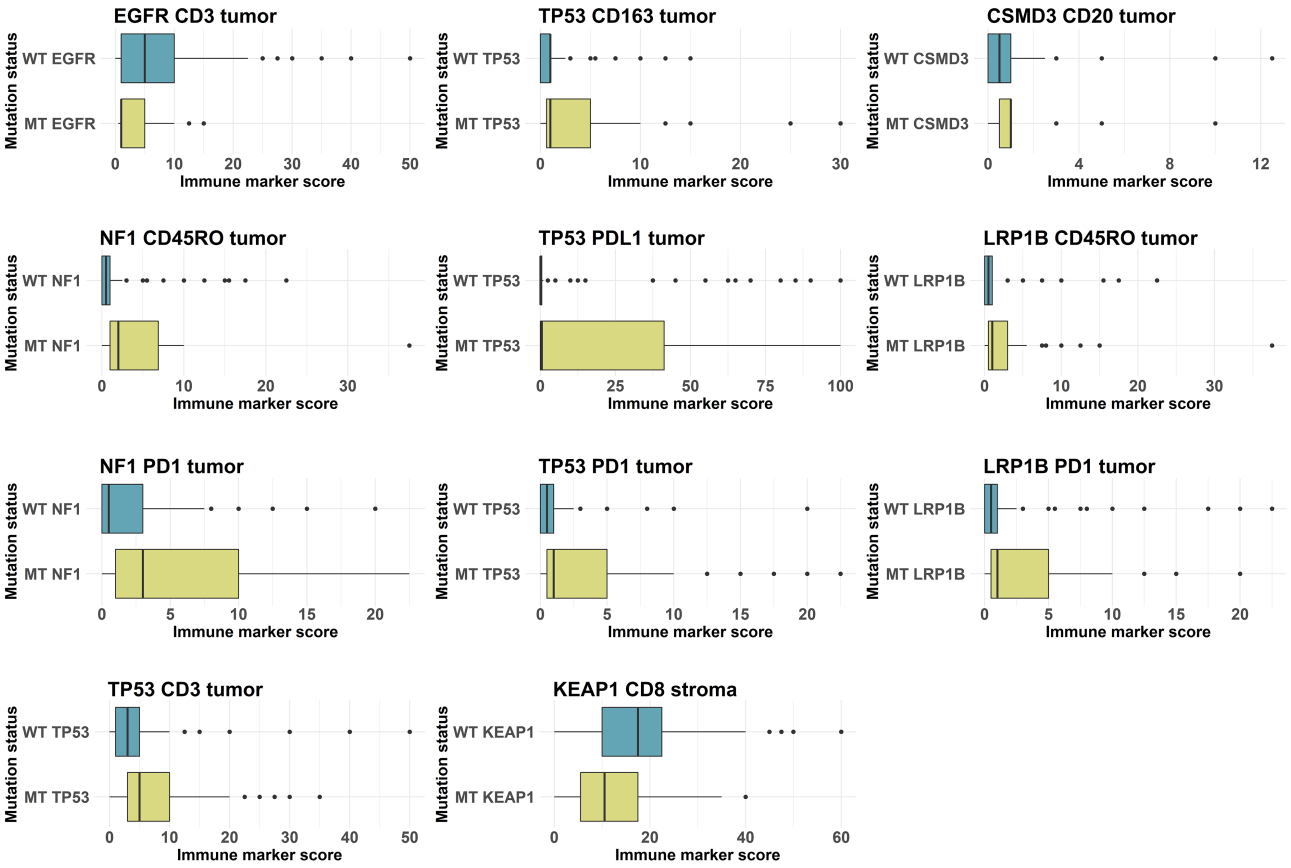

Figure 2. Relationship of mutation status to immune marker score in adenocarcinoma. The mutation status of the targeted sequence analysis (82 genes) was associated with compartment-specific immune cell infiltration or PD1 and PD-L1 expression. The figure shows mutations that were significantly associated with a distinct immune infiltration in adenocarcinomas (see also supplementary material, Table S5C). No associations were seen in the squamous cell carcinoma subgroup (see supplementary material, Table S5D). MT, mutated; WT, wild type.

DESeq2 version 3.12. The top 100 most differentially expressed genes between each group were included in a gene ontology analysis directly on the Gene Ontology Consortium website (geneontology.org) using the PANTHER classification system [27].

P values < 0.05 were considered to be significant and adjustment for multiple testing was carried out using the Benjamini–Hochberg procedure within each histology group (all NSCLC, adenocarcinoma, and squamous cell cancer). All analyses, if not otherwise indicated, were performed using R version 4.0.2.

Results

Immune cell infiltration in NSCLC

NSCLC tissue from 357 operated patients (Table 1) were stained for lymphocytic markers (CD3, CD4, CD8, CD20, FOXP3, CD45RO), anti-inflammatory macrophages/myeloid cells (CD163), plasma cells (CD138), NK cells (NKp46), and the checkpoint molecule PD-L1, as well as PD1. CD163 was chosen as a tumor-associated macrophage marker because our previous analyses showed a high correlation between the pan-macrophage marker CD68 and CD163, a marker for anti-inflammatory macrophages [28]. The markers were annotated as the percentages of stained viable cells in the tumor and stroma compartments separately. Representative examples are shown in Figure 1A. The protein expression based on IHC markers pooled for tumoral and stromal compartments correlated well with the RNAseq expression of the corresponding genes (see supplementary material, Figure S1). Only NKp46+ (NK cells) and CD138+ cells (plasma cells) did not show a significant correlation. For NKp46, this was probably due to low cell abundance. The discrepancy related to CD138 can be explained by the fact that CD138 is expressed on plasma cells but also on tumor and bronchial epithelial cells, which were excluded in the IHC annotation. The results support the validity of the analyzed markers and the reliability of the IHC-based annotation.

In principle, all immune cells showed a higher abundance in the stroma compartment than in the tumor compartment (see supplementary material, Figure S2 and Table S3) The single most abundant cell type in the stroma were CD163+ cells, i.e. anti-inflammatory macrophages/myeloid cells, often considered to represent M2 macrophages [29].

In the tumor compartment, the most frequent immune cells were CD3+ T cells. Within this group, CD8+ cells

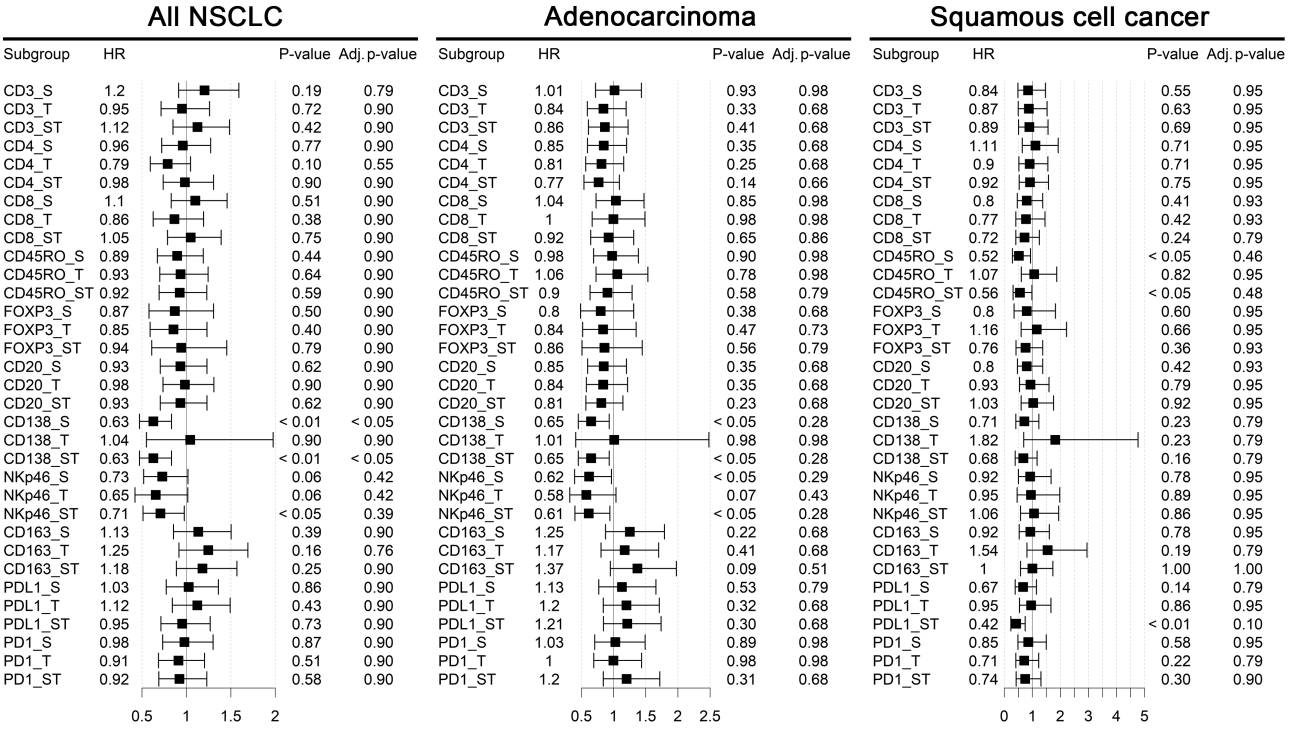

Figure 3. Association of immune infiltration with overall survival. A Cox regression model was applied to analyze the association of the immune marker scores in all NSCLC, adenocarcinoma, and squamous cell cancer for tumor and stroma compartments. The hazard ratio of each association is displayed in the forest plots. S, stroma; T, tumor; ST, stroma and tumor taken together as a total score. The Cox regression model was controlled for age, stage, smoking, and performance status (*P* value). *P* values were also adjusted for multiple testing (adj. *P* value).

(cytotoxic T cells) showed a higher predilection for tumor infiltration than CD4+ cells (T helper cells) and CD163+ cells. Notably, FOXP3+ (T regulatory cells) and CD138+ cells (plasma cells) were rarely identified in the tumor compartment, while relatively abundant in the stroma. PD-L1 expression demonstrated the expected proportions, with 55% negative cases, 45% cases with ≥1, and 17% of cases with ≥50% positive tumor cells. A generic NSCLC immune cell profile, based on the average abundance of each cell type and marker, in the tumor and stroma compartments, respectively, is illustrated in Figure 1B.

The pattern of immune cell infiltration was different between the main histologic subtypes of NSCLC (see supplementary material, Table S3). In the stroma, adenocarcinoma showed a higher infiltration of all T cell subtypes except FOXP3+ regulatory T cells, whereas plasma cells and NK cells were more abundant in squamous cell cancer (all adjusted $p < 0.05$). In the tumor cell compartment, CD20+ cells were more frequent in adenocarcinoma and CD45RO+ cells were more frequent in squamous cell cancer. Thus, the immune response is influenced by the histologic subtype of NSCLC.

Immune cell correlations

To identify possible associations between different immune cell types, we correlated the annotation scores for all immune cells to each other. This was carried out for all NSCLC cases, as well as for adenocarcinoma and squamous cell cancer separately (see supplementary material, Table S4A–C). There was a strong cross-correlation of immune scores, indicating a coordinated immune cell infiltration. Thus, if one immune cell type was present, other immune cell types were also likely to be present. This was true for the immune cell infiltration of the tumor as well as the stroma compartment and was particularly pronounced for the lymphocytic subpopulations. Also, high PD-L1 expression of tumor cells or inflammatory cells in the stromal compartment correlated with high immune cell infiltrates; in particular, CD8+, CD45RO+, FOXP3+, CD163+, and NKp46+ cells.

Immune cell infiltration in relation to mutations

Targeted sequencing of 82 cancer-related genes was performed on 352 of the 357 NSCLC patients. Genes that were mutated in at least 10% of samples were included in the subsequent analysis (see supplementary material, Table S9) with the aim of evaluating if specific genetic alterations in tumor cells are linked to a specific immune reaction (see supplementary material, Table S5B–D). Associations of specific immune cell markers were in principle only seen in the histologic subset of adenocarcinomas (see supplementary material, Table S5C) and concerns *KEAP*, *NF1*, *LRP1B*, *CSMD3*, *EGFR*, and *TP53* mutations (Figure 2). *TP53* mutations showed the most frequent associations to immune cell infiltration. *TP53*-mutated tumors showed higher number of CD3+ and CD163+ cells in the tumor compartment and were more often PD-L1 positive. A particularly

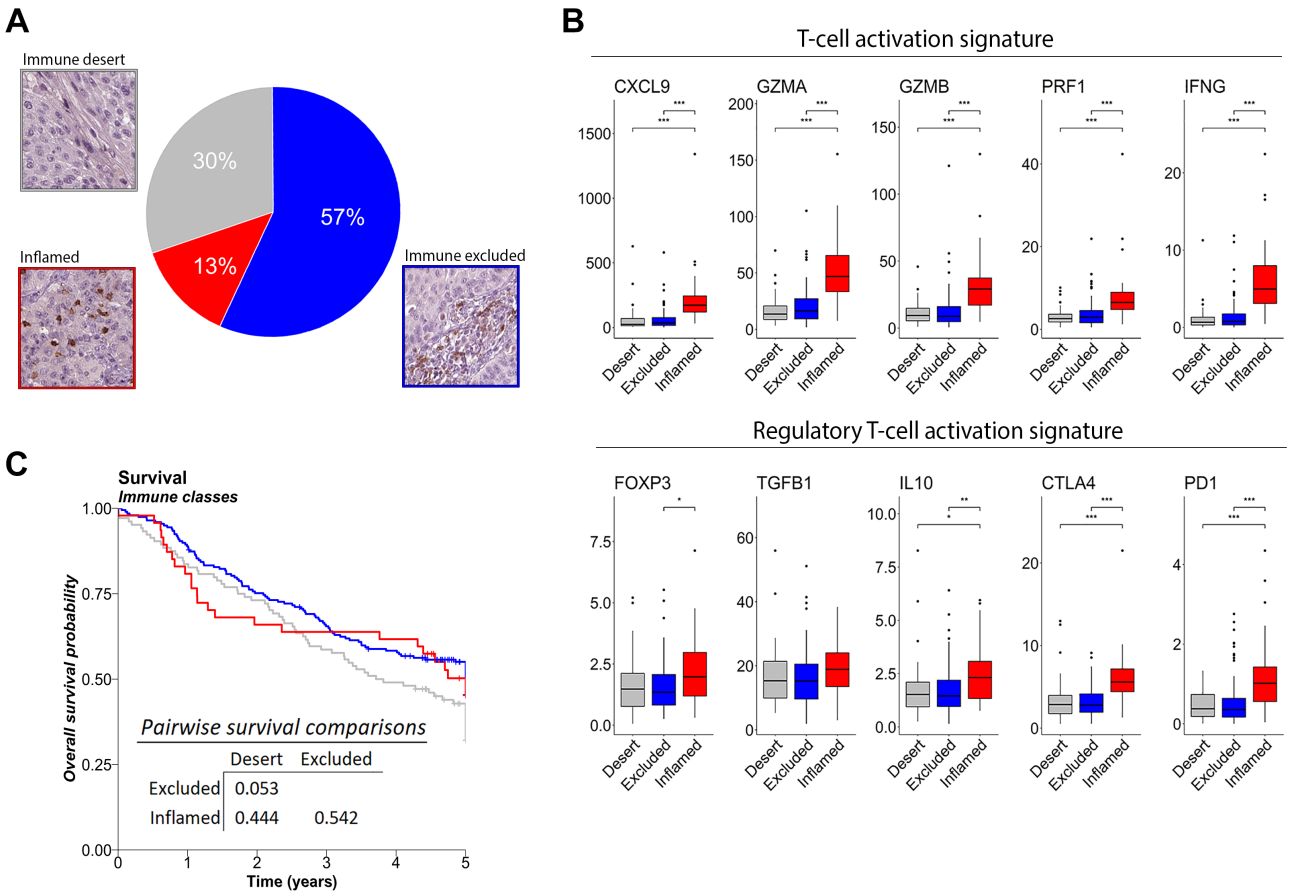

Figure 4. CD8-based immune phenotypes in NSCLC. (A) The number and distribution of CD8+ cells were used to assign 350 patients to the immune classes inflamed, immune excluded, and desert. (B) The immune classes were analyzed regarding the expression of genes associated with T cell activation and regulation based on RNAseq data that were available for 195 cases. $^{*}p < 0.05$, $^{**}p < 0.001$, $^{***}p < 0.0001$. (C) Kaplan–Meier plots show the survival of patients according to the three immune classes.

strong association (adjusted $p = 0.00001$) was observed between the presence of *TP53* mutations and high PD1+ cell infiltrates in the tumor compartment. No relations between immune cells and mutation were identified when the smaller subgroup of squamous cell cancer was analyzed (see supplementary material, Table S5D).

Finally, we estimated the total TML based on the targeted sequencing data. In the analysis of adenocarcinomas, a higher estimated TML was associated with a higher proportion of CD8+ and CD45RO+ cells in the tumor compartment, higher FOXP3+ cells in the stroma compartment, as well as higher CD163+ cells in the tumor and the stroma compartment. The estimated TML was also associated with higher PD-L1 tumor cell expression. Furthermore, the TML correlated strongly with PD1+ immune cells in both the tumor and stroma compartments (both adjusted $p < 0.001$). No correlation between estimated TML and immune infiltration in the smaller squamous cell cancer subgroups was noted (see supplementary material, Table S5A).

Overall, the results indicate that the genetic background of the tumor, in terms of acquired somatic mutations and estimated TML, is of relevance for the immune microenvironment of NSCLC.

Immune cell infiltration, clinical correlates, and survival

The abundance of immune cells was correlated to dichotomized clinical parameters: age, performance status, gender, smoking status, and stage (see supplementary material, Table S6). No statistically significant correlation was observed after adjustment for multiple testing (false discovery rate > 0.05); neither for the whole cohort nor for either of the main histologic subgroups. The strongest trend (false discovery rate $= 0.11$) was seen in ever-smokers, which revealed higher numbers of CD163+ cells and PD1+ cells in the tumor compartment. If all evaluated correlations were taken into consideration, a trend was apparent for immune cells of any subtype: more frequent in female patients, smokers, younger patients, and patients with a better performance status or a lower stage.

The immune cell infiltration scores were then tested for correlation with overall survival, as illustrated in the forest plots (Figure 3). Controlled for age, stage, performance status, and smoking, total tumor infiltration (stroma and tumor area combined) of NK and plasma cells was associated with longer survival in the complete

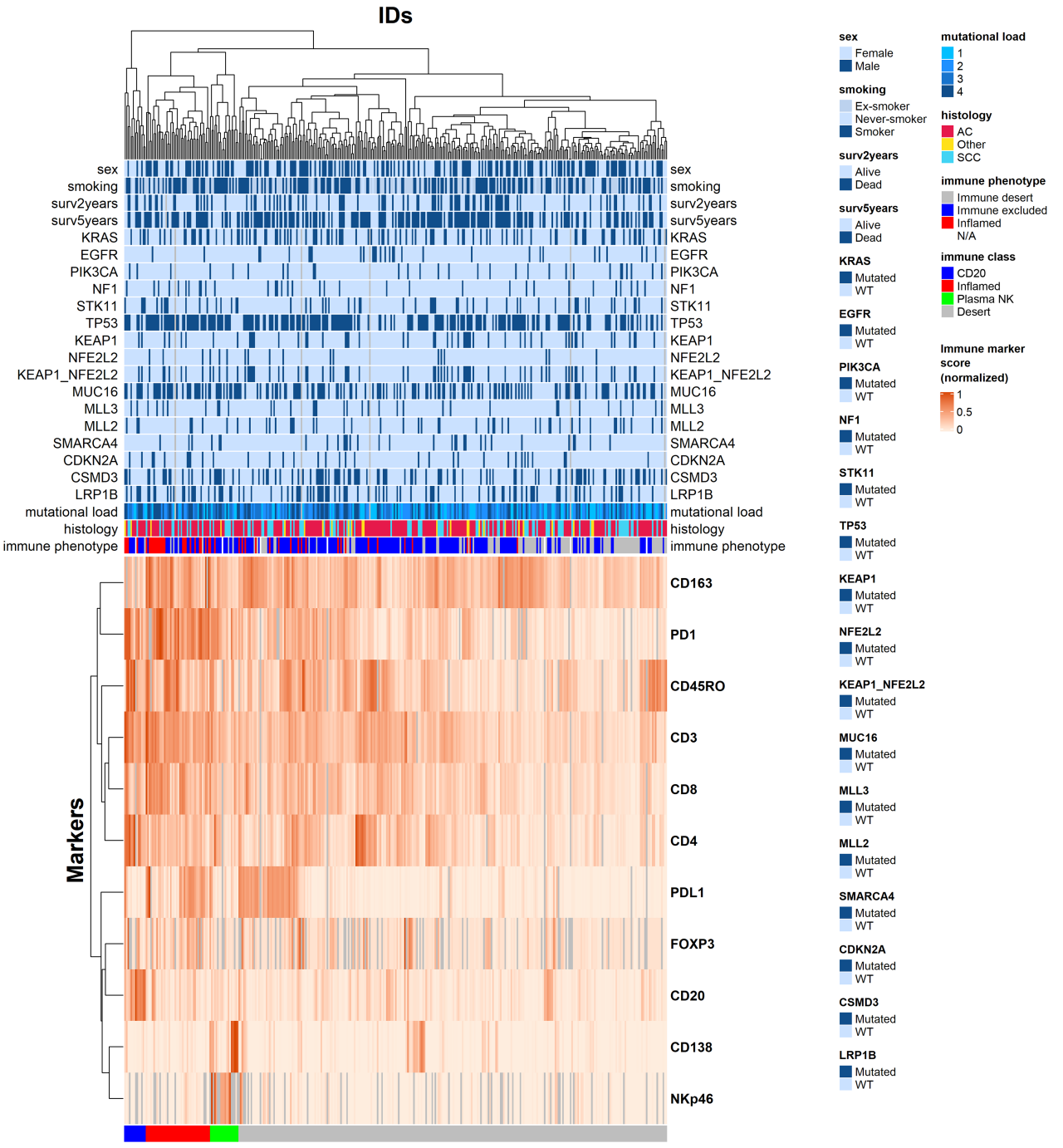

Figure 5. Unsupervised hierarchical cluster analysis of immune markers in the tumor compartment. NSCLC cases (357) were clustered, based on the levels of immune marker scores and proportion of PD-L1 expression in the tumor compartment. The upper rows specify sex, smoking status, 2- and 5-year survival, as well as mutation status, estimated TML, and main histologic subtype, as well as the assignment to the immune phenotypes inflamed, immune excluded, or desert. The lowest row of the figure illustrates the four defined immune classes.

cohort and in the adenocarcinoma subgroup. In squamous cell cancer, PD-L1 expression and CD45RO+ cell infiltration was associated with longer survival. Thus, the prognostic impact of immune profiles seems to be histology dependent, in part reflecting the findings that the immune cell infiltration patterns were different in adenocarcinoma and squamous cell cancer.

However, these associations should be interpreted with caution. After strict adjustment for multiple testing, only plasma cell infiltration remained significantly associated with survival in the complete NSCLC cohort.

T cell-based immune classification of NSCLC

Three histologically distinct immune patterns have been described to represent natural occurring cancer immunity: inflamed, desert, and immune excluded (Figure 4A) [30]. We captured these immune phenotypes using the

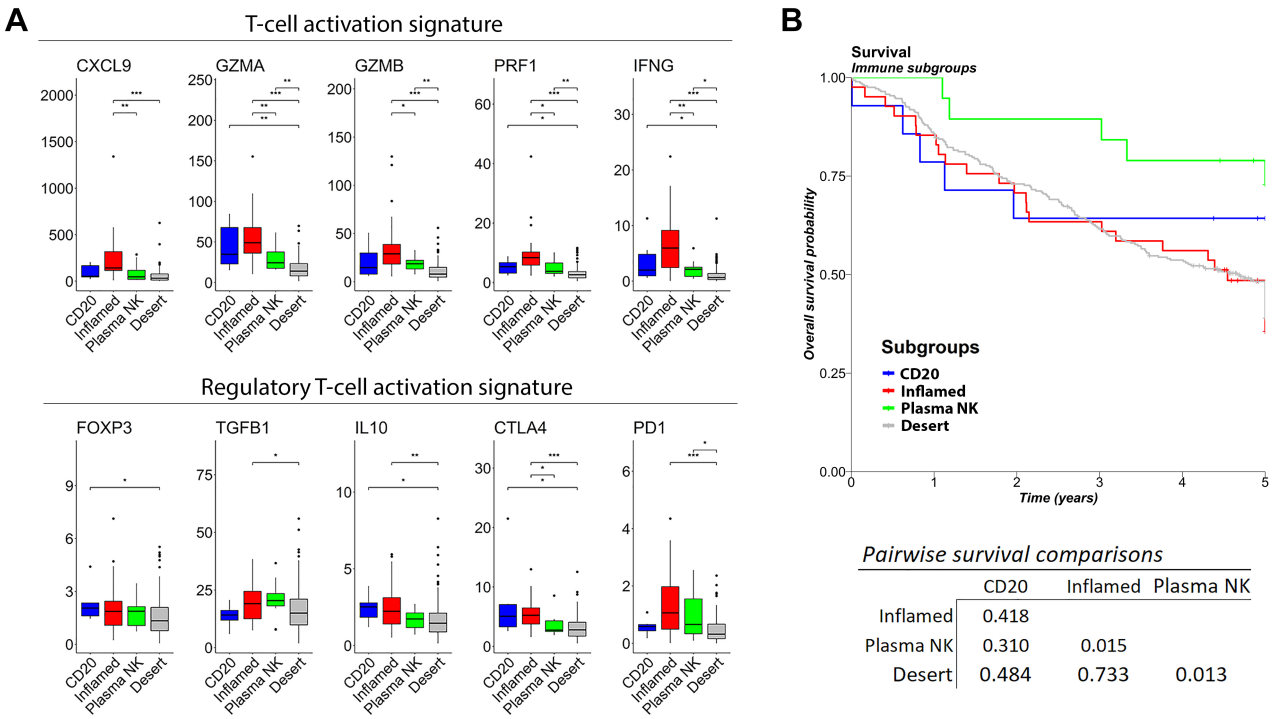

Figure 6. (A) Expression levels of T cell-related genes in the immune classes. RNAseq data were available for 197 cases of the Uppsala II cohort. The four immune classes derived from the cluster analysis were compared with regard to the mRNA expression (FPKM values) of genes-related T cell activation and T cell regulation. $^{*}p < 0.05$, $^{**}p < 0.001$, $^{***}p < 0.0001$. (B) Survival analysis of immune classes. Kaplan–Meier analysis of the four immune classes (CD20, inflamed, plasma NK, and desert) were based on the cluster analysis of the immune marker scores of the complete NSCLC cohort. The table gives the *P* values of the pairwise comparisons of overall survival.

proportion of CD8 infiltrates in the stroma and tumor compartments. Most cases (57%) were characterized by an abundance of CD8 lymphocytes in the stroma but low direct infiltration in the tumor compartment, designated as immune excluded. Only 13% of cases demonstrated a typical inflamed phenotype, with high CD8 cells in the tumor compartment. By contrast, 30% showed an immune desert pattern, with low CD8 cell infiltration in both tissue compartments. For a subset of 190 patients, we compared gene expression profiles between the three immune classes. Only the inflamed group showed a distinct upregulation of genes associated with T cell activation (*CXCL9*, *GZMA*, *GZMB*, *PRF1*, *INFG*) and T cell regulation (*FOXP3*, *TGFB1*, *IL10*, *CTLA4*, *PDCD1*/PD1) (Figure 4B). Similarly, differential expression analysis indicated a general higher expression of immune-related markers in the inflamed phenotype than in the excluded/desert phenotype (see supplementary material, Table S10A–C). Notably, these upregulated genes were related to the gene ontology terms 'positive regulation of NK cell-mediated immunity'. Moreover, cases in the inflamed group revealed a significantly higher estimated TML than cases in the excluded or desert subsets (see supplementary material, Table S7A). There was no difference in the frequency of specific mutations (see supplementary material, Table S8A) but there were more squamous cell cancer subtypes in the desert group (see supplementary material, Table S7C). Finally, we compared overall survival between the three immune classes, and observed a non-significant but clear trend towards better survival of the excluded phenotype compared with the desert subset ($p = 0.053$) (Figure 4C).

Taken together, only the inflamed group revealed a specific immune response pattern associated with higher mutational load, still without any impact on survival. These results indicate that a simplistic classification based on CD8 cells may not reflect the complexity of the immune response against cancer, at least not in the natural course of tumor development in naïve non-treated patients.

Extension of immune phenotypes in NSCLC

In order to investigate if the explanatory power of immune phenotypes could be improved, we applied an unbiased approach and included all 11 immune markers in an unsupervised hierarchical cluster analysis. The heat map for immune cell infiltration and immune markers revealed four main clusters (Figure 5). The largest cluster comprised 282 cases with general lower numbers of immune cells, a group that overlapped partially with the previously described desert pattern [9,29]. Two other clusters showed overall high immune cell counts ($n = 42$), differing mainly in the abundance of CD20+ cells ($n = 14$). Finally, a small cluster ($n = 19$) was distinguished with a relative abundance of the NKp46+ (NK cells) and/or CD138+ cells (plasma cells). We designated this group plasma NK.

For further characterization we compared the available RNAseq data for each group (desert, inflamed, CD20, and plasma NK). Differential gene expression analysis revealed typical motifs associated with the immune cell type in general (supplementary material, Table S11). In line with lymphocyte infiltration data, T cell activation and regulatory genes showed significantly lower expression levels in the desert groups than in all other groups (Figure 6).

Neither the frequency of specific mutations, the estimated TML nor the proportion of histologic subtypes were different between the four immune classes in the complete NSCLC cohort (see supplementary material, Tables S7B,D and S8B).

Finally, the survival analysis demonstrated that the plasma NK subclass was linked to significantly better survival, with a 5-year survival rate of 73% versus 39% in the desert subgroup and 36% in the inflamed group (Figure 6). The analysis of the clinical characteristics (age, sex, smoking status, histology, stage, performance status) of the patients in this plasma NK cell group revealed no significant difference compared with the rest of the patient cohort (see supplementary material, Table S12).

Discussion

Our study provides a comprehensive description of the immune landscape of NSCLC based on immune cell infiltration *in situ* and gene expression profiles, analyzed in connection with the detailed mutational background of a large clinical patient cohort. The study supplements previous efforts to understand the immune response in NSCLC and also extends current concepts of immune classifications.

Previous immune classifications were mainly based on lymphocytic infiltration, with focus on CD8+ T cells. Based on microscopical quantification of cell infiltrates in the tumor cell compartment and the surrounding stroma, three patterns (inflamed, desert, and excluded) have been proposed to reflect distinct tumor-associated immunoreactivity patterns [9,12,30,31]. However, the applied criteria to define these patterns differ considerably regarding the amount and type of immune cells, as well as location, that are used for categorization [10,32,33]. To our knowledge, this is the first time that this concept has been rigorously applied on a large cohort of lung cancer samples.

In our study, most cases showed an immune excluded phenotype with immune infiltration that was restricted to the stroma. Despite abundant immune cells, the T cell activation status based on gene expression profiles did not reveal a significant difference between the immune excluded and desert phenotypes. This indicates an effective silencing of the immune response and supports the assumption that both phenotypes represent functionally non-inflamed tumors.

Only a few tumors revealed the classical inflamed phenotype with increased expression of T cell activation markers (INFG and granzyme A) and a concurrent upregulation of inhibiting signals (e.g. PD1), which is in accordance with T cell exhaustion [34,35]. Surprisingly, the three immune patterns did not reflect responses with bearing on survival in the natural course of NSCLC. Notably, this does not exclude an influence, when checkpoint inhibitor therapy is used to relieve T cell inhibition in treated patients.

By contrast, when we used an unbiased strategy and included more immune cells and markers into the analysis, a different, partially overlapping pattern emerged. We identified an immune cluster comprising around 5% of cases with a signature of NK cells and/or plasma cells. This subgroup showed favorable prognosis, even though markers of T cells and their activation were low. This finding is reflected by the fact that only the presence of NK and plasma cells was associated with long-term survival in the uni- and multivariate Cox regression models.

How does the presence of NK and plasma cells contribute to the favorable prognosis? It has been shown that plasma cells present the cell type with the strongest association with long-term survival in many cancer types, including lung cancer [36–39]. Plasma cells are often present at sites of inflammation and are generated from activated B cells by T cell-dependent and -independent mechanisms. T cell-independent responses lead to the production of natural Ig isotypes (IgM and IgA) and do not require help from previous antigen presentation. The T cell-dependent mechanism requires antigen presentation and concomitant T cell activation in secondary lymphoid organs leading to Ig isotype switch (IgA, IgG, IgE). It would therefore be interesting to explore Ig isotype patterns in plasma cell-rich tumors. As antigen presentation and T cell-dependent B cell activation occur in secondary lymphoid organs, it is not possible to say whether the plasma cells present in tumors are there as a consequence of previous T cell-dependent B cell activation or not. Of note, recently the presence of tertiary lymphoid structures in melanoma tumors with potential intra-tumoral activation of B cells has been proposed as an important predictive marker for immune checkpoint blockade [40].

NK cells represent an effective innate immune cell population with tumoricidal capacity that does not require previous antigen presentation and activation in lymph nodes [41]. Infiltration of tumors by NK cells has been linked to a favorable outcome, although the studies in lung cancer are limited [42,43]. NK cells can kill cancer cells through different mechanisms, including death receptors, cytotoxicity by exocytosis of granules, and cytokine release, and in addition they are involved in the regulation of other immune cells.[44] The low RNA expression of perforin and granzyme A/B in this plasma NK group may indicate that the NK cells are exhausted, but one may also speculate that they have switched to death receptor-dependent mechanisms involving the activation of caspase cascades [45]. The infiltration by NK and plasma cells may be coincidental. However, several lines of evidence suggest a crosstalk

between NK and B cells. In particular, NK cells may stimulate B cell maturation toward a plasma cell phenotype with associated Ig production [46,47]. In addition, plasma cells produce Igs against tumor cell epitopes and enables anti-tumoral NK cell-mediated antibody-dependent cellular cytotoxicity (mediated either via granzyme release or death receptors). The interaction of CD40 ligand on activated NK cells with its receptor on B cells seems to be the main molecular mechanism for the NK–B cell crosstalk [47,48]. It is conceivable to speculate that the NK–plasma cell immune profile reflects a favorable activation status of the host immunity, manifested by NK and plasma cells. This would extend the previously described role of NK cells in cancer immunity [44]. In melanoma, the abundance of NK cells correlates with overall survival in the TCGA datasets and the responsiveness to anti-PD1 immune checkpoint therapy [48]. Further evaluation of the NK–plasma cell class and related immune cell populations is clearly warranted, to confirm our observations and critically test alternative interpretations.

Another novel group that our cluster analysis revealed was characterized by abundant inflammatory cells and B cell infiltration (CD20). Because this group included few cases, it was difficult to carry out a statistically meaningful comparative analysis for further characterization. Therefore, although interesting, we regard this finding as descriptive.

To our knowledge, there are only a few previous studies that have analyzed a broader spectrum of immune cells in the tumor microenvironment of lung cancer in relation to clinical and molecular data. Most studies have focused on the T lymphocytes and macrophages, and not included plasma cells or NK cells [49]. Kadara *et al* [50] analyzed 10 immune markers (PD-L1, PD1, CD3, CD4, CD8, CD45RO, CD57, CD68, FOXP3, and granzyme B) in a cohort of 92 lung adenocarcinomas in relation to whole exome sequencing data. They found a decreased CD4/CD8 expression in tumors with *STK11* mutations and higher PD-L1 expression in tumors with *TP53* mutations.

Another study evaluated 221 adenocarcinomas with respect to the markers CD68 (monocyte/macrophage), CD66 (neutrophilic granulocyte marker), CD8 (cytotoxic lymphocytes), and LAMP3 (dendritic cell marker) [51]. In a cluster analysis they defined three clusters: (1) inflamed with dominant lymphocytic infiltration; (2) infiltration mainly by macrophages; and (3) poor immune cell infiltration. The inflamed cluster showed a strong trend for longer survival compared with both other groups. The authors also observed that the inflamed group had more *TP53* mutations but fewer *STK11* mutations. Our cluster analysis did not support these relationships. Instead, we found that *TP53* mutant tumors showed a higher infiltration of CD163+ cells and CD3+ cells, also indicating a more inflamed tumor type. We could not show a link between *STK11* mutations and immune cells, possibly due to the small subgroup size. Independent studies are required to evaluate whether our strict adjustment for multiple testing in the statistical analysis leads to an underestimation of correlations between immune infiltrations and mutation patterns.

A previous study included our patient cohort to describe the prognostic impact of immune markers in 705 patients [25]. Although the main results were provided on a merged data set, the prognostic impact of the immune markers of our cohort was given separately. In agreement with our study, it displayed a general trend that higher numbers of immune cells were associated with longer survival. Only CD79A (B cell marker) and IGKC (plasma cell marker) were significantly associated with longer survival. In the present study, although we used CD138 instead of IGKC as a plasma cell marker, we found the same strong association between survival and plasma cell infiltration. This indicates the reliability of the semiquantitative assessment of IHC staining of immune cells and that the strong associations are independent of the observer.

Our study is hitherto the most comprehensive regarding the number of immune markers, molecular parameters, and annotation complexity included in the analyses of lung cancer. However, some aspects should be taken into consideration when interpreting our results. As we used TMAs, the whole tissue section was represented by only two 1-mm cores. Thus, we cannot fully capture the tissue heterogeneity and could potentially miss certain immune cellular compartments, such as tertiary lymphoid structures that are considered to play a central role in cancer immunity [40,52]. Furthermore, the quantification and localization of cell types were made based on microscopic evaluation on separate sections. Thus, cell distances and interaction were not assessed. More recent multiplex techniques with automated quantifications would provide a more accurate quantification and spatial information [53,54].

Also, because of the retrospective nature of our study, the data can only be related to clinical development after surgery and other second-line modalities of treatment available during the time period up to 2010. An entirely different picture may emerge when the response to immunotherapy is studied. On the other hand, our data suggest interesting new perspectives to consider when evaluating immunotherapy responses. We believe that it is worthwhile to include markers, especially for plasma and NK cells, in prospective studies of immune checkpoint inhibitors.

In conclusion, our study provides a detailed, compartment-specific description of immune infiltrates in NSCLC. The findings extend previous concepts and suggest that specific attention to plasma cells and NK cells is warranted. Further refinement of the immune classification will hopefully provide better tools to guide therapy or suggest alternative treatment strategies to overcome resistance to immunotherapy.

Acknowledgements

We acknowledge our colleague and good friend Ennio Carbone who passed away during the preparation of this

manuscript. He was substantially involved in the study design, analysis, and interpretation of the data.

This study was partly supported by the Swedish Cancer Society, the Lions Cancer Foundation Uppsala, Sweden, the Swedish Government Grant for Clinical Research, the Mrs. Berta Kamprad Foundation, Sweden, The Swedish Medical Research Council, and the Sjöberg Foundation, Sweden. We thank the Research and Development Unit of the Uppsala Pathology Department for technical assistance.

Author contributions statement

MB, LLF, DD and JSSM performed most of the experimental procedures. PM, JB, AM, KK, KL, SM, CL and MB conceived and designed the study, PM, JB, MG, KJ and MB carried out the histological review of the cases. PMI, DD, JSSM, FP, KJ and HB helped to create the TMAs. MB, LLF, PK, DD, HE, JSSM and ME annotated the staining. PMI reviewed all annotations. JI, JM, DD and PM helped to compile the clinical data. MB, CS, AM and VP performed or assisted with the statistical analyses. MB, LLF, KK, FP, JB, SM, KL, CS and PM wrote the original draft. MB, CS, KK, KL, CS, JI, JB and PM revised the final version.

Data availability statement

Raw data, together with clinical information, are available on the gene expression omnibus with the accession number GSE81089 (https://www.ncbi.nlm.nih.gov/geo/query/acc.cgi?acc=GSE81089).

References

1. Sanmamed MF, Eguren-Santamaria I, Schalper KA. Overview of lung cancer immunotherapy. *Cancer J* 2020; **26:** 473–484.
2. Brahmer J, Reckamp KL, Baas P, *et al*. Nivolumab versus docetaxel in advanced squamous-cell non-small-cell lung cancer. *N Engl J Med* 2015; **373:** 123–135.
3. Garon EB, Rizvi NA, Hui R, *et al*. Pembrolizumab for the treatment of non-small-cell lung cancer. *N Engl J Med* 2015; **372:** 2018–2028.
4. Socinski MA, Jotte RM, Cappuzzo F, *et al*. Atezolizumab for first-line treatment of metastatic nonsquamous NSCLC. *N Engl J Med* 2018; **378:** 2288–2301.
5. Carbone DP, Reck M, Paz-Ares L, *et al*. First-line nivolumab in stage IV or recurrent non-small-cell lung cancer. *N Engl J Med* 2017; **376:** 2415–2426.
6. Herbst RS, Soria JC, Kowanetz M, *et al*. Predictive correlates of response to the anti-PD-L1 antibody MPDL3280A in cancer patients. *Nature* 2014; **515:** 563–567.
7. Gettinger SN, Choi J, Mani N, *et al*. A dormant TIL phenotype defines non-small cell lung carcinomas sensitive to immune checkpoint blockers. *Nat Commun* 2018; **9:** 3196.
8. Zhang Q, Luo J, Wu S, *et al*. Prognostic and predictive impact of circulating tumor DNA in patients with advanced cancers treated with immune checkpoint blockade. *Cancer Discov* 2020; **10:** 1842–1853.
9. Chen DS, Mellman I. Elements of cancer immunity and the cancer-immune set point. *Nature* 2017; **541:** 321–330.
10. Milette S, Fiset PO, Walsh LA, *et al*. The innate immune architecture of lung tumors and its implication in disease progression. *J Pathol* 2019; **247:** 589–605.
11. Galon J, Mlecnik B, Bindea G, *et al*. Towards the introduction of the 'Immunoscore' in the classification of malignant tumours. *J Pathol* 2014; **232:** 199–209.
12. Fehrenbacher L, Spira A, Ballinger M, *et al*. Atezolizumab versus docetaxel for patients with previously treated non-small-cell lung cancer (POPLAR): a multicentre, open-label, phase 2 randomised controlled trial. *Lancet* 2016; **387:** 1837–1846.
13. Karasaki T, Nagayama K, Kuwano H, *et al*. An immunogram for the cancer-immunity cycle: towards personalized immunotherapy of lung cancer. *J Thorac Oncol* 2017; **12:** 791–803.
14. Chae YK, Pan A, Davis AA, *et al*. Biomarkers for PD-1/PD-L1 blockade therapy in non-small-cell lung cancer: is PD-L1 expression a good marker for patient selection? *Clin Lung Cancer* 2016; **17:** 350–361.
15. Lizotte PH, Ivanova EV, Awad MM, *et al*. Multiparametric profiling of non-small-cell lung cancers reveals distinct immunophenotypes. *JCI Insight* 2016; **1:** e89014.
16. Spranger S, Gajewski TF. A new paradigm for tumor immune escape: β-catenin-driven immune exclusion. *J Immunother Cancer* 2015; **3:** 43.
17. Spranger S, Luke JJ, Bao R, *et al*. Density of immunogenic antigens does not explain the presence or absence of the T-cell-inflamed tumor microenvironment in melanoma. *Proc Natl Acad Sci U S A* 2016; **113:** E7759–E7768.
18. Faruki H, Mayhew GM, Serody JS, *et al*. Lung adenocarcinoma and squamous cell carcinoma gene expression subtypes demonstrate significant differences in tumor immune landscape. *J Thorac Oncol* 2017; **12:** 943–953.
19. Maleki Vareki S. High and low mutational burden tumors versus immunologically hot and cold tumors and response to immune checkpoint inhibitors. *J Immunother Cancer* 2018; **6:** 157.
20. Galon J, Costes A, Sanchez-Cabo F, *et al*. Type, density, and location of immune cells within human colorectal tumors predict clinical outcome. *Science* 2006; **313:** 1960–1964.
21. Micke P, Mattsson JS, Djureinovic D, *et al*. The impact of the fourth edition of the WHO classification of lung tumours on histological classification of resected pulmonary NSCCs. *J Thorac Oncol* 2016; **11:** 862–872.
22. Mattsson JS, Brunnström H, Jabs V, *et al*. Inconsistent results in the analysis of ALK rearrangements in non-small cell lung cancer. *BMC Cancer* 2016; **16:** 603.
23. La Fleur L, Falk-Sörqvist E, Smeds P, *et al*. Mutation patterns in a population-based non-small cell lung cancer cohort and prognostic impact of concomitant mutations in KRAS and TP53 or STK11. *Lung Cancer* 2019; **130:** 50–58.
24. Djureinovic D, Hallström BM, Horie M, *et al*. Profiling cancer testis antigens in non-small-cell lung cancer. *JCI Insight* 2016; **1:** e86837.
25. Edlund K, Madjar K, Mattsson JSM, *et al*. Prognostic impact of tumor cell programmed death ligand 1 expression and immune cell infiltration in NSCLC. *J Thorac Oncol* 2019; **14:** 628–640.
26. Gu Z, Eils R, Schlesner M, *et al*. EnrichedHeatmap: an R/Bioconductor package for comprehensive visualization of genomic signal associations. *BMC Genomics* 2018; **19:** 234.
27. Mi H, Muruganujan A, Casagrande JT, *et al*. Large-scale gene function analysis with the PANTHER classification system. *Nat Protoc* 2013; **8:** 1551–1566.
28. La Fleur L, Boura VF, Alexeyenko A, *et al*. Expression of scavenger receptor MARCO defines a targetable tumor-associated macrophage subset in non-small cell lung cancer. *Int J Cancer* 2018; **143:** 1741–1752.

29. La Fleur L, Botling J, He F, *et al*. Targeting MARCO and IL37R on immunosuppressive macrophages in lung cancer blocks regulatory T cells and supports cytotoxic lymphocyte function. *Cancer Res* 2021; **81:** 956–967.
30. Hegde PS, Karanikas V, Evers S. The where, the when, and the how of immune monitoring for cancer immunotherapies in the era of checkpoint inhibition. *Clin Cancer Res* 2016; **22:** 1865–1874.
31. Mariathasan S, Turley SJ, Nickles D, *et al*. TGFβ attenuates tumour response to PD-L1 blockade by contributing to exclusion of T cells. *Nature* 2018; **554:** 544–548.
32. Hegde PS, Chen DS. Top 10 challenges in cancer immunotherapy. *Immunity* 2020; **52:** 17–35.
33. Kockx MM, McCleland M, Koeppen H. Microenvironmental regulation of tumour immunity and response to immunotherapy. *J Pathol* 2021; **254:** 374–383.
34. Cai MC, Zhao X, Cao M, *et al*. T-cell exhaustion interrelates with immune cytolytic activity to shape the inflamed tumor microenvironment. *J Pathol* 2020; **251:** 147–159.
35. Cheng H, Ma K, Zhang L, *et al*. The tumor microenvironment shapes the molecular characteristics of exhausted $CD8^+$ T cells. *Cancer Lett* 2021; **506:** 55–66.
36. Gentles AJ, Newman AM, Liu CL, *et al*. The prognostic landscape of genes and infiltrating immune cells across human cancers. *Nat Med* 2015; **21:** 938–945.
37. Schmidt M, Hellwig B, Hammad S, *et al*. A comprehensive analysis of human gene expression profiles identifies stromal immunoglobulin κ C as a compatible prognostic marker in human solid tumors. *Clin Cancer Res* 2012; **18:** 2695–2703.
38. Lohr M, Edlund K, Botling J, *et al*. The prognostic relevance of tumour-infiltrating plasma cells and immunoglobulin kappa C indicates an important role of the humoral immune response in non-small cell lung cancer. *Cancer Lett* 2013; **333:** 222–228.
39. Tsou P, Katayama H, Ostrin EJ, *et al*. The emerging role of B cells in tumor immunity. *Cancer Res* 2016; **76:** 5597–5601.
40. Cabrita R, Lauss M, Sanna A, *et al*. Tertiary lymphoid structures improve immunotherapy and survival in melanoma. *Nature* 2020; **577:** 561–565.
41. Dianat-Moghadam H, Mahari A, Heidarifard M, *et al*. NK cells-directed therapies target circulating tumor cells and metastasis. *Cancer Lett* 2021; **497:** 41–53.
42. Takanami I, Takeuchi K, Giga M. The prognostic value of natural killer cell infiltration in resected pulmonary adenocarcinoma. *J Thorac Cardiovasc Surg* 2001; **121:** 1058–1063.
43. Villegas FR, Coca S, Villarrubia VG, *et al*. Prognostic significance of tumor infiltrating natural killer cells subset CD57 in patients with squamous cell lung cancer. *Lung Cancer* 2002; **35:** 23–28.
44. Paul S, Lal G. The molecular mechanism of natural killer cells function and its importance in cancer immunotherapy. *Front Immunol* 2017; **8:** 1124.
45. Prager I, Liesche C, van Ooijen H, *et al*. NK cells switch from granzyme B to death receptor-mediated cytotoxicity during serial killing. *J Exp Med* 2019; **216:** 2113–2127.
46. Katz P, Whalen G, Cupps TR, *et al*. Natural killer cells can enhance the proliferative responses of B lymphocytes. *Cell Immunol* 1989; **120:** 270–276.
47. Blanca IR, Bere EW, Young HA, *et al*. Human B cell activation by autologous NK cells is regulated by CD40-CD40 ligand interaction: role of memory B cells and CD5+ B cells. *J Immunol* 2001; **167:** 6132–6139.
48. Carbone E, Ruggiero G, Terrazzano G, *et al*. A new mechanism of NK cell cytotoxicity activation: the CD40-CD40 ligand interaction. *J Exp Med* 1997; **185:** 2053–2060.
49. Bremnes RM, Al-Shibli K, Donnem T, *et al*. The role of tumor-infiltrating immune cells and chronic inflammation at the tumor site on cancer development, progression, and prognosis: emphasis on non-small cell lung cancer. *J Thorac Oncol* 2011; **6:** 824–833.
50. Kadara H, Choi M, Zhang J, *et al*. Whole-exome sequencing and immune profiling of early-stage lung adenocarcinoma with fully annotated clinical follow-up. *Ann Oncol* 2017; **28:** 75–82.
51. Biton J, Mansuet-Lupo A, Pécuchet N, *et al*. TP53, STK11, and EGFR mutations predict tumor immune profile and the response to anti-PD-1 in lung adenocarcinoma. *Clin Cancer Res* 2018; **24:** 5710–5723.
52. Sautès-Fridman C, Petitprez F, Calderaro J, *et al*. Tertiary lymphoid structures in the era of cancer immunotherapy. *Nat Rev Cancer* 2019; **19:** 307–325.
53. Mezheyeuski A, Bergsland CH, Backman M, *et al*. Multispectral imaging for quantitative and compartment-specific immune infiltrates reveals distinct immune profiles that classify lung cancer patients. *J Pathol* 2018; **244:** 421–431.
54. Decalf J, Albert ML, Ziai J. New tools for pathology: a user's review of a highly multiplexed method for *in situ* analysis of protein and RNA expression in tissue. *J Pathol* 2019; **247:** 650–661.

SUPPLEMENTARY MATERIAL ONLINE

Supplementary figure legends

Figure S1. Correlation between IHC annotations and RNAseq

Figure S2. Pattern of immune cell infiltrates and PD-L1

Table S1. Haloplex gene panel and mean read depth in target genes [23]

Table S2. Patient characteristics of the subgroup with available RNAseq data

Table S3. Comparison of immune infiltration and PD-L1 in adenocarcinoma and squamous cell cancer

Table S4A. Cross-correlation of immune cell score as well as PD-L1 expression in stroma and tumor compartments in all non-small cell lung cancers

Table S4B. Cross-correlation of immune infiltration and PD-L1 expression in stroma and tumor compartments in adenocarcinomas

Table S4C. Cross-correlation of immune infiltration and PD-L1 expression in stroma and tumor compartments in squamous cell carcinoma

Table S5A. Correlations between the estimated tumor mutational load (TML) and immune infiltrates in the tumor (T) and the stroma (S) for all NSCLC cases as well as both major histologic subgroups; adenocarcinoma (AC) and squamous cell cancer (SCC)

Table S5B. Association between mutational status and immune infiltrates and PD-L1 in all non-small cell lung cancer cases

Table S5C. Association between mutational status and immune infiltrates and PD-L1 in adenocarcinoma

Table S5D. Association between mutational status and immune infiltrates and PD-L1 in squamous cell cancer

Table S6. Association between clinical parameters (dichotomized) and immune cell score and PD-L1 in the tumor or stroma compartment

Table S7A. Comparison of estimated tumor mutational load (TML) between the immune classes (inflamed, excluded, desert)

Table S7B. Comparison of the tumor mutational load (TML) between immune classes (inflamed, CD20, plasma NK, and desert)

Table S7C. Comparison of histologic subtypes between immune classes (inflamed, excluded, desert)

Table S7D. Comparison of histologic subtypes between immune classes (inflamed, CD20, plasma NK, and desert)

Table S8A. Comparison of mutation frequency between different immune classes (inflamed, excluded, desert)

Table S8B. Comparison of mutation frequency between different immune classes (CD20, inflamed, plasma NK, and desert)

Table S9. Mutation frequencies in 21 genes selected for further analysis

Table S10A. Differential gene expression analysis of inflamed immune class versus excluded and desert

Table S10B. Differential gene expression analysis of excluded immune class versus inflamed and desert

Table S10C. Differential gene expression analysis of desert class versus inflamed and desert

Table S11A. Differential gene expression analysis of CD20 immune class versus inflamed, plasma NK, and desert

Table S11B. Differential gene expression analysis of the inflamed immune class versus CD20, plasma NK, and desert

Table S11C. Differential gene expression analysis of plasma NK immune class versus CD20, inflamed, and desert

Table S11D. Differential gene expression analysis of desert immune class versus CD20, inflamed, and plasma NK

Table S12. Clinical parameters of patients assigned to the four different immune classes